Supplementary Information

An optofluidic "tweeze-and-drag" cell stretcher in a microfluidic channel

Zhanshi Yao, Ching Chi Kwan and Andrew W. Poon*

Photonic Device Laboratory, Department of Electronic and Computer Engineering, The Hong Kong University of Science and Technology, Clear Water Bay, Hong Kong SAR, China.
E-mail: eeawpoon@ust.hk

S1. Flipping of RBCs in an optical tweezer

We employ the three-dimensional finite-element method (FEM) in COMSOL Multiphysics to numerically calculate the torque on an oblate-shape cell from an optical tweezer. Figure S1(a) shows schematically an oblate-shape cell trapped by an optical tweezer in a buffer solution in the Cartesian coordinate system. The cell shape is rotationally symmetric about its polar axis (minor axis), which is shorter than its equatorial axis (major axis). In order to calculate the torque on the cell at different orientations, we rotate the cell about one of its equatorial axis in the x direction with a rotation angle ϕ varying from 0° to 360°. We define ϕ = 0° when the polar axis of the cell is in the y direction. We set the major axis of the cell to be 7.5 μm and the minor axis to be 4 μm. We set an optical tweezer with the beam waist positioned at the centre of the cell and along the z axis. We assume a wavelength of 1064 nm and a beam waist diameter at 1/e of the maximum amplitude of 0.8 μm. We set an optical power to be 25 mW and a polarization along the transverse x axis. The refractive indices of the cell and the buffer solution are 1.378 and 1.335, respectively.

Figure S1(b) shows the simulated electric field amplitude distribution in the y-z plane when x = 0 and rotation angle ϕ = 0°. After obtaining the field distribution, we extract the optical stress at the cell surface using the Maxwell stress tensor $\overleftrightarrow{T}$:[1,2]

$$\vec{\sigma} = \left(\overleftrightarrow{T}_2 - \overleftrightarrow{T}_1\right) \cdot \vec{n} = \frac{\varepsilon_0}{2}(n_1^2 - n_2^2)\left[\left(\frac{n_1^2}{n_2^2}\right)E_n^2 + E_t^2\right]\vec{n}$$

where $\overleftrightarrow{T}_1$ and $\overleftrightarrow{T}_2$ are the Maxwell stress tensors in the cell and in the buffer solution, respectively, $\vec{n}$ is the unit normal vector of the cell surface, ε_0 is the vacuum permittivity, E_n and E_t are the normal and tangential components of the electric field, respectively. Figures S1(c)-S1(f) show the extracted optical stress vector-field distributions at the cell surface in the y-z plane when x = 0 and ϕ = 0°, 30°, 60°, and 90°. For each cell surface element, we calculate the torque as:

$$\Delta\overleftrightarrow{\tau} = \vec{r} \times \vec{\sigma}$$

where $\vec{r} = (x, y, z)$ is the position vector and $\vec{\sigma} = (\sigma_x, \sigma_y, \sigma_z)$ is the optical stress. The x component of the torque is

$$\Delta\tau_x = y\sigma_z - z\sigma_y$$

We calculate the x component of the total torque on the cell by integrating $\Delta\tau_x$ over the cell surface:

$$\tau_x = \oiint \Delta\tau_x dS$$

Figures S1(g) shows the calculated x component of the torque as a function of rotation angle. A positive τ_x rotates the cell in the counter-clockwise direction. We calculate the rotational potential U as

$$U = \int_0^{\phi} \tau_x d\phi$$

Figure S1(h) shows the rotational potential U as a function of rotation angle. We show that cell reaches a stable equilibrium at rotation angles of 0°, 180° and 360°, where the polar axis of the cell is transverse to the beam axis.

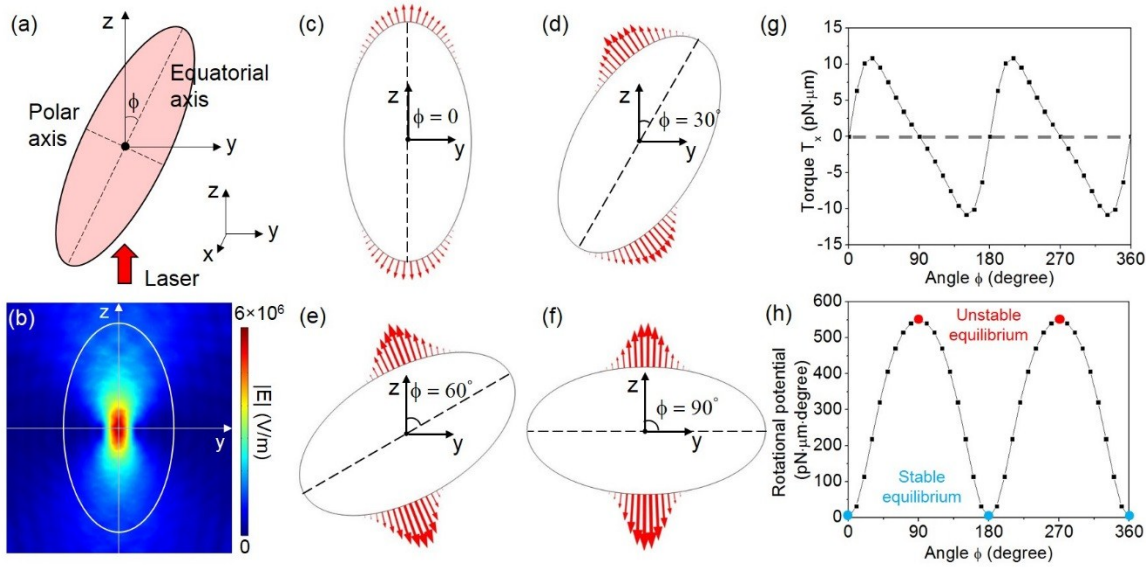

Fig. S1 (a) Schematic of an oblate cell trapped by an optical tweezer. (b) Simulated electric field amplitude distribution in the y-z plane when x = 0 and ϕ = 0. (c)-(f) Simulated optical stress vector-field distributions at the cell surface at rotation angles of (c) 0°, (d) 30°, (e) 60° and (f) 90°. (g) Calculated x component of the torque (τ_x) as a function of rotation angle. (h) Calculated rotational potential as a function of rotation angle.

S2. Microfluidic channel fabrication

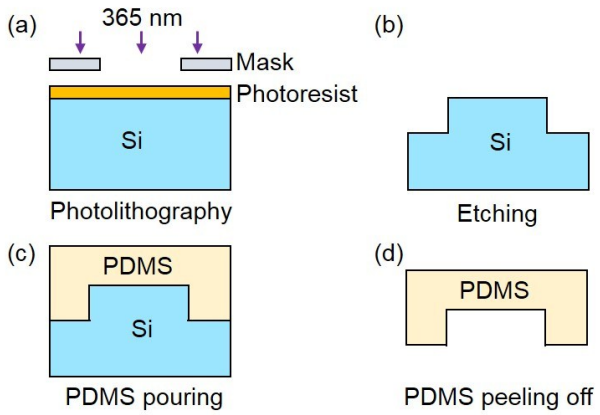

Fig. S2 Fabrication process flow for the PDMS microfluidic channel layer based on a soft-lithography process. (a) i-line photolithography on a bare silicon wafer. (b) Deep reactive-ion etching to transfer the microfluidic channel patterns onto the silicon wafer. The etching depth is ~40 μm. (c) PDMS is poured onto the etched silicon wafer with a thickness of ~3 mm. The silicon wafer is used as a mould. (d) The PDMS layer is peeled off from the mould.

S3. Chopping frequency

Figure S3(a) shows the sequential video frames of an RBC interacting with the optical tweezer with an optical power of 25 mW and a flow rate of 2.5 µl/hr at a chopping rate of 2 Hz. The cell requires ~ 0.1 s to be fully re-oriented and aligned with the flow. Figure S3(b) shows the sequential video frames of an RBC under the same test condition but at a chopping rate of 5 Hz. The cell cannot be fully re-oriented with an interaction time shorter than 0.1 s.

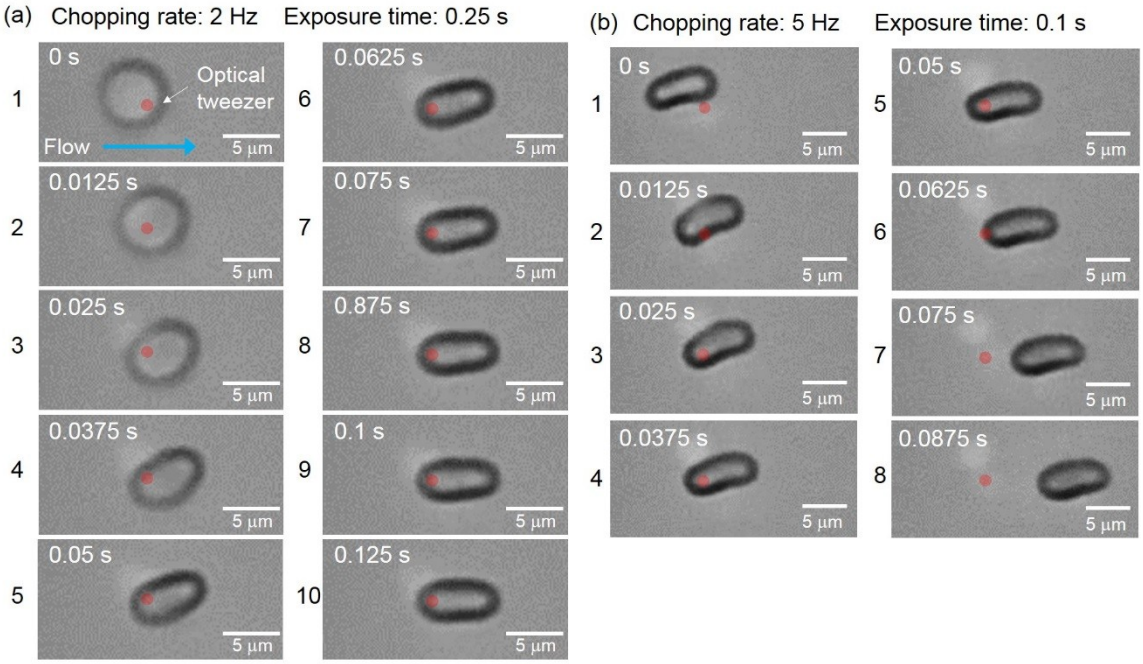

Fig. S3 (a) Images of a cell trapped by the optical tweezer with an optical power of 25 mW and a flow rate of 2.5 µl/hr at a chopping rate of ~ 2 Hz. (b) Images of a cell trapped by the optical tweezer under the same test condition but at a chopping rate of ~ 5 Hz.

S4. Image processing

We use a program to process the recorded video frames based on the Image Processing Toolbox and the Computer Vision System Toolbox in Matlab. The image processing mainly comprises three steps including (i) edge detection, (ii) object segmentation and (iii) feature extraction. Figure S4(a) shows the top-view optical micrograph of an RBC. Figure S4(b) shows a binary mask that contains the edge profile of the cell and some irrelevant edges from the cell image in Fig. S4(a) in the edge detection step. Each pixel of the binary mask corresponds to actual dimensions of $x_p = y_p = 0.166$ μm. Figure S4(c) shows a filled binary mask that represents the profile of the detected cell in the object segmentation step. Figure S4(d) shows the measurements of the centroid position (x, y), the major axis (d_{maj}) and the minor axis (d_{min}) of the detected cell profile in the feature extraction step.

Using the extracted centroid positions of the cells in each video frame, we track the cell trajectories and measure the speed of the cells. Figure S4(e) shows the images of three sequential frames illustrating the tracking of three different cells by finding the cells with the closest locations in adjacent frames. The speed of the cell is calculated by: speed = $\Delta x/\Delta t$, where Δx is the change of the x position of the cell between two adjacent frames and Δt is the time interval between two adjacent frames.

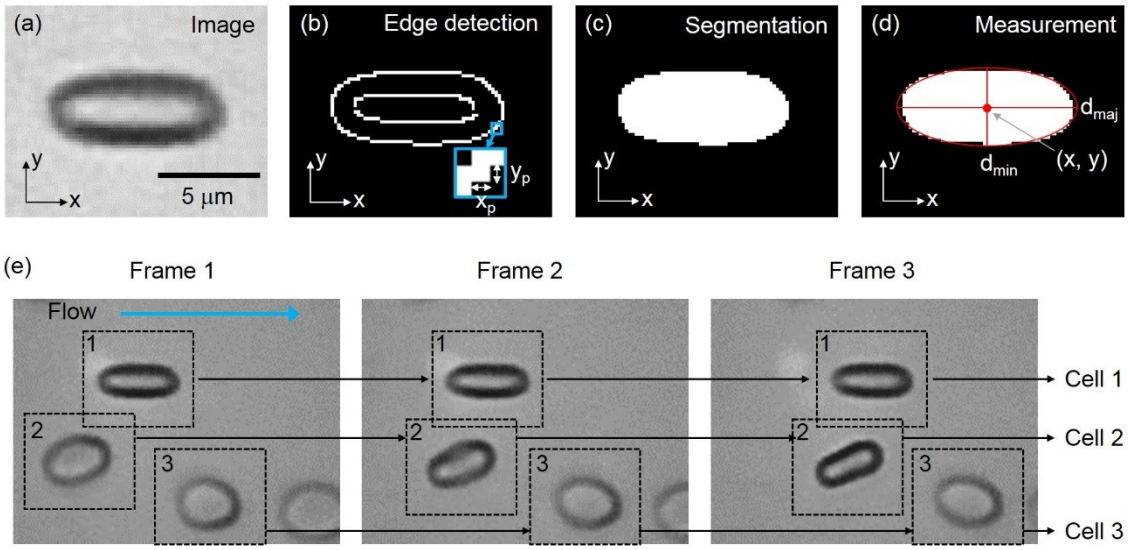

Fig. S4 (a) A top-view optical micrograph of an RBC. (b) A binary mask containing the edge profile of the cell image in (a) created in the edge detection step. Each pixel of the binary mask corresponds to actual dimensions of $x_p = y_p = 0.166$ μm. (c) A binary mask representing the cell profile created in the object segmentation step. (d) Parameter measurements assuming the cell follows an ellipsoidal shape. (e) Images of three sequential frames illustrating the tracking of three different cells by finding the cells with the closest locations in adjacent frames.

S5. Finding the speed threshold for removing un-trapped cells

Figure S5(a) shows the zoom-in view of the speed distribution shown in Fig. 3(b) near the trapping region. We indicate the speed of 20 μm/s using a gray dashed line. Figures S5(b)-S5(d) show the trajectories of the cells after applying different speed thresholds of 100 μm/s, 60 μm/s and 20 μm/s.

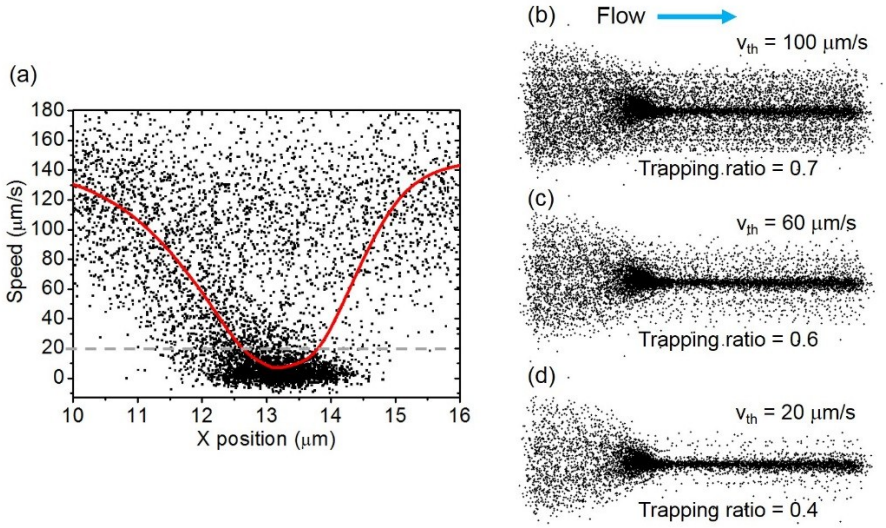

Fig. S5 (a) Zoom-in view of the speed distribution shown in Fig. 3(b) near the trapping region. (b)-(d) Trajectories of the cells after applying different speed thresholds of (b) 100 μm/s, (c) 60 μm/s and (d) 20 μm/s.

S6. Calculation of the fluidic drag force on a thin disk

Figure S6(a) shows schematically a thin circular disk with a diameter d of 7.5 μm in the x-y plane. A flow streams through the disk with a uniform velocity U in the x direction and is parallel to the plane of the disk. We set the dynamic viscosity of the fluid to be $\eta = 10^{-3}$ N·m^{-2}·s and the density ρ to be 10^3 kg/m^3. With U = 200 μm/s, the Reynolds number is

$$Re = \frac{\rho d U}{\eta} \approx 1.5 \times 10^{-3} \ll 1$$

The flow is in the low-Reynolds-number regime, and thus we can describe the flow using the Stokes equations assuming an incompressible fluid[3,4]

$$\eta \nabla^2 \vec{v} - \nabla p = 0$$

$$\nabla \cdot \vec{v} = 0$$

where $\vec{v}$ is the local velocity and p is the local pressure. Assuming a no-slip condition, we have $v_x = v_y = v_z$ at the disk surface. At infinity, we have $v_x = U$ and $v_y = v_z = 0$. Applying these boundary conditions to the Stokes equations, we can solve for the distribution of the velocity field $\vec{v}$.[4]

Figures S6(b) and S6(c) show the calculated distributions of the velocity fields in the x-y plane and in the x-z plane, respectively. The stress components acting on the surface of the disk are[3,4]

$$\sigma_{31} = \eta\left(\frac{\partial v_x}{\partial z} + \frac{\partial v_z}{\partial x}\right) = \frac{8\eta U}{3\pi\sqrt{(d/2)^2 - r^2}}$$

$$\sigma_{32} = \eta\left(\frac{\partial v_y}{\partial z} + \frac{\partial v_z}{\partial y}\right) = 0$$

$$\sigma_{33} = -p + 2\eta\frac{\partial v_z}{\partial z} = -p_0$$

where σ_{31}, σ_{32} and σ_{33} are stress components in the x, y and z directions, respectively, r is the distance to the disk centre, and p_0 is a constant fluid pressure that is not related with the flow speed.

Figure S6(d) shows the calculated distribution of σ_{31} in the x-y plane. We calculate the fluidic drag force acting on the disk by integrating σ_{31} on both sides of the disk: [3,4]

$$F_x = 2\int_0^{2\pi}\int_0^{d/2} \sigma_{31} r dr d\phi = \frac{16\eta d U}{3}$$

Assuming a flow speed of U = 200 μm/s, we estimate the total fluidic drag force on the disk to be ~8 pN, which is sufficient to induce shape deformations of RBCs.

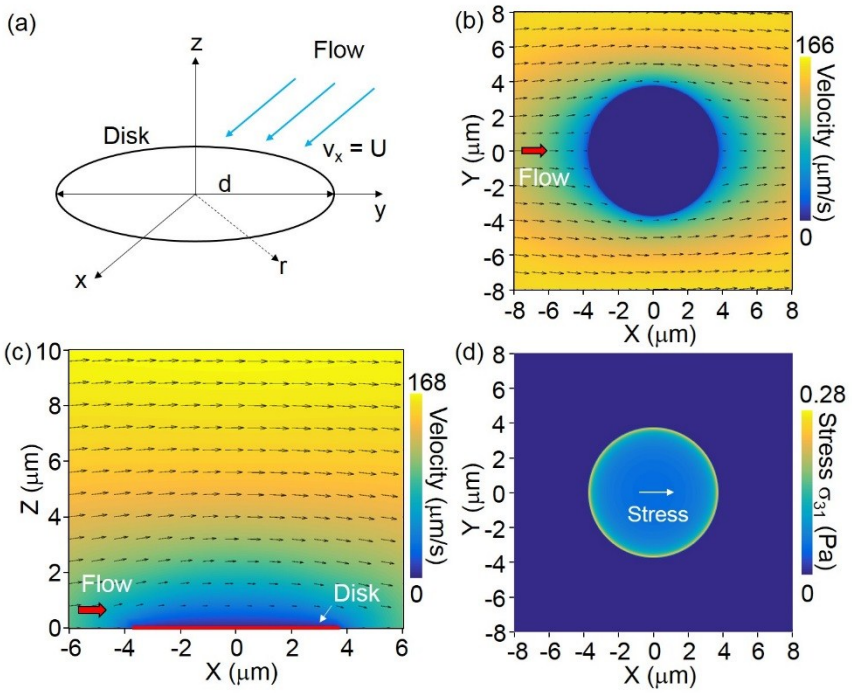

Fig. S6 (a) Schematic of a thin circular disk in the x-y plane and a flow streaming through with a uniform velocity in the x direction. (b)-(c) Calculated distributions of the velocity fields (b) in the x-y plane and (c) in the x-z plane. (d) Calculated distribution of stress component σ_{31} in the x-y plane.

S7. Estimation of the optical force on the cell

To estimate the optical force on the trapped disk-shape RBCs, we employ the three-dimensional FEM in COMSOL Multiphysics to numerically calculate the optical force exerted by an optical tweezer on an oblate-shape cell (Fig. S7(a)).

The simulation parameters follow those detailed in section "S1. Flipping of RBCs in an optical tweezer". The cell shape is rotationally symmetric about its polar axis (minor axis), which is shorter than its equatorial axis (major axis). When the cell is tweezed by the optical tweezer and dragged by the flow, the cell is reoriented such that the surface normal of the flat surface is transverse to both the beam propagation direction (z) and the flow direction (x).

In the simulation, we vary the displacement Δx between the RBC center and the optical tweezer beam waist position from –5 μm to 5 μm, as illustrated in Fig. S7(a). We calculate at various Δx values (with an interval of 0.25 μm) the optical field distributions and the associated optical stress distributions on the cell surface.

Figure S7(b) shows the simulated electric field amplitude distribution in the x-z plane when Δx = 0. Figures S7(c)-(f) show the extracted optical stress vector-field distributions at the cell surface in the x-z plane when Δx = 0 μm, 2 μm, 4 μm and 4.5 μm.

We extract the resulting optical force components in the transverse x direction (F_x) and in the longitudinal z direction (F_z) by integrating the calculated optical stress over the cell surface. Figure S7(g) shows the calculated F_x and F_z as a function of Δx. We observe that F_x dominates F_z with 0 μm < $|\Delta x|$ < 5 μm. The maximum F_x is ~ 14 pN at $|\Delta x|$ = 3.5 μm. The F_x acts as a restoring force when the cell is displaced from the equilibrium position of Δx = 0 μm.

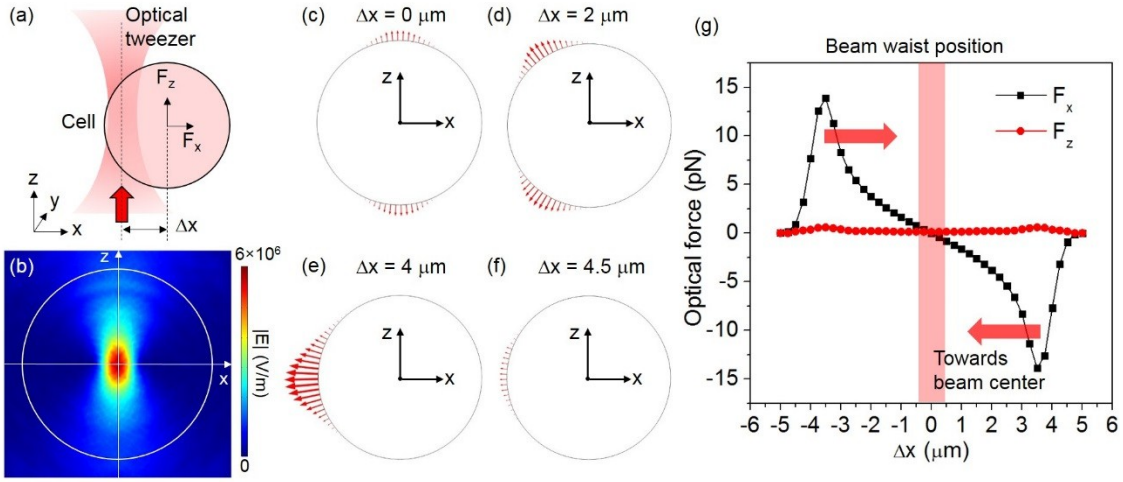

Fig. S7 (a) Illustration of the disk-shape cell displaced from the tweezer by Δx in the x-z plane . (b) Simulated electric field amplitude distribution in the cell in the x-z plane when Δx = 0 μm. (c)-(f) Simulated optical stress vector-field distributions at the cell surface in the x-z plane with (c) Δx = 0 μm, (d) Δx = 2 μm, (e) Δx = 4 μm, and (f) Δx = 4.5 μm. (g) Calculated optical force components in the x direction (F_x) and in the z direction (F_z) as a function of Δx.

S8. Stretching of spherical RBCs

Figure S8(a) shows the microscope images of an osmotically swollen RBC tweezed and dragged in our stretcher. Figure S8(b) shows the measured cell length change as a function of the escaped cell speed (proportional to the fluidic drag force) for healthy RBCs (untreated) and RBCs treated with glutaraldehyde with a concentration of ~0.002%. We extract the corresponding spring constants for the healthy swollen RBCs to be 12 ± 2 μN/m and for the treated swollen RBCs to be 20 ± 3 μN/m.

We calibrate the optical force by trapping a cell in a static condition then we increase the fluidic flow until the cell is released from the tweezer. We estimate the maximum optical force to be 8 ~ 11 pN upon an optical power of ~25 mW (using a microscope objective lens with an NA of 0.85) by measuring the velocity of the escaped cell and calculating the fluidic drag force based on the Stokes' law. The measured optical force is consistent with our estimated optical force based on the numerical simulation in section "S7. Estimation of the optical force on the cell".

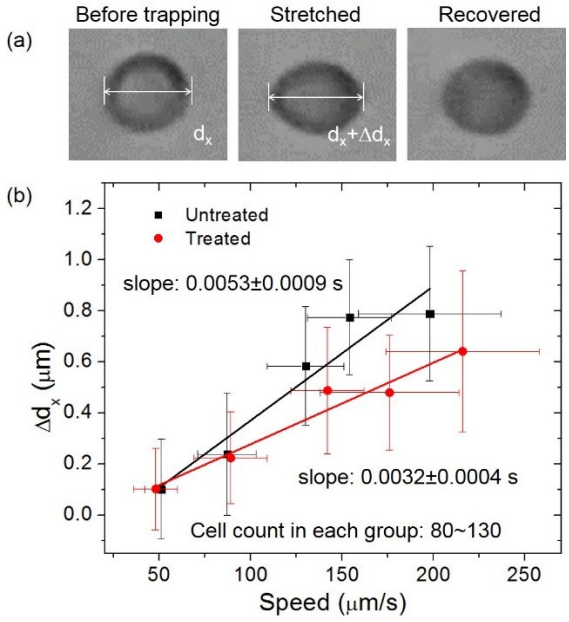

Fig. S8 (a) Microscope images of an osmotically swollen RBC in a spherical shape tweezed and dragged in our cell stretcher. (b) Measured cell length change as a function of the escaped cell speed for healthy RBCs (untreated) and RBCs treated with glutaraldehyde with a concentration of ~0.002%.

S9. Cell stretching with an optical power of 45 mW

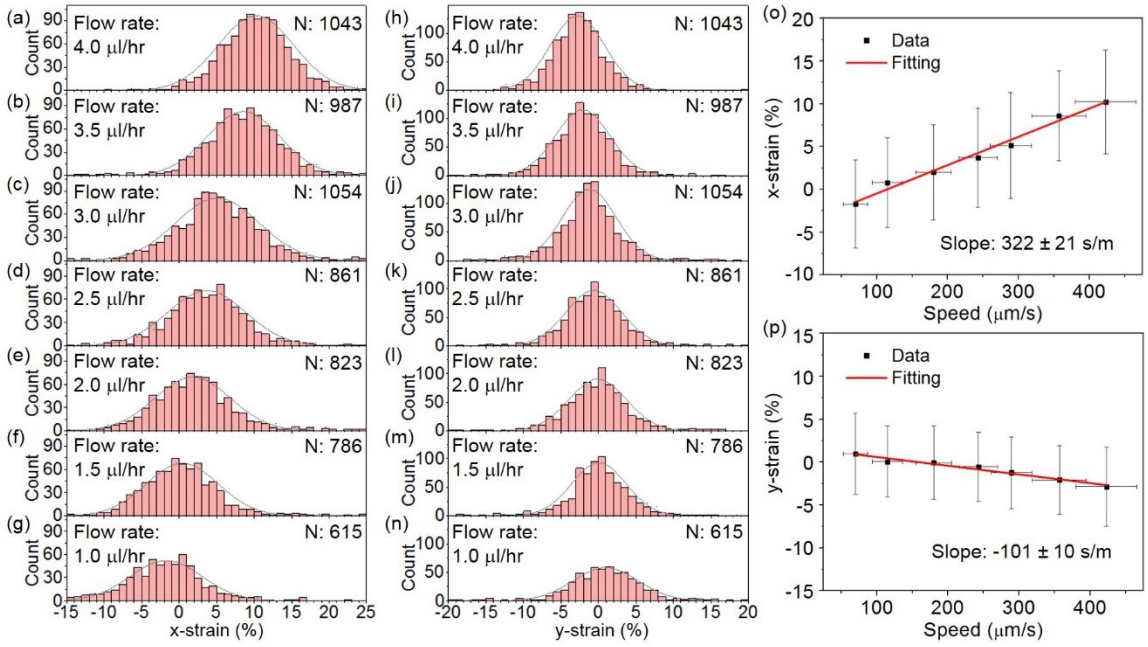

Fig. S9 (a)-(g) Histograms of the distributions of x-strain upon an optical power of 45 mW and flow rates of (a) 4 μl/hr, (b) 3.5 μl/hr, (c) 3 μl/hr, (d) 2.5 μl/hr, (e) 2 μl/hr, (f) 1.5 μl/hr and (g) 1 μl/hr. (h)-(n) Histograms of the distributions of y-strain upon an optical power of 45 mW and flow rates of (h) 4 μl/hr, (i) 3.5 μl/hr, (j) 3 μl/hr, (k) 2.5 μl/hr, (l) 2 μl/hr, (m) 1.5 μl/hr and (n) 1 μl/hr. (o) x-strain and (p) y-strain with cell escape speed. The linear fits indicate the slopes to be 322 ± 21 s/m and -101 ± 10 s/m, respectively.

References

1. J. D. Jackson, Classical Electrodynamics, Wiley, 1998.
2. L. Yu, Y. Sheng, and A. Chiou, Three-dimensional light-scattering and deformation of individual biconcave human blood cells in optical tweezers, Opt. Express, 2013, **21**, 12174-12184.
3. J. Happel, H. Brenner, Low Reynolds number hydrodynamics: with special applications to particulate media. Springer Science & Business Media, 2012
4. M. Ray, Application of Bessel functions to the solution of problem of motion of a circular disk in viscous liquid, Phil. Mag., 1936, 21, 546-564.